Density Functional Theory Investigation of Decamethyldizincocene

James W. Kress

7630 Salem Woods Drive, Northville, Michigan 48167

Received: March 2, 2005; In Final Form: June 17, 2005

A density functional investigation into the structure and vibrational properties of the recently synthesized, novel, Zn(I)-containing species decamethyldizincocene has been performed. Our analysis is in agreement with the general structural properties of the experimental results. We have corroborated the experimental geometry as a true minimum on the global molecular energy surface, confirmed the experimental hypothesis that the Zn atoms are in a Zn(I) state, and provided a detailed analysis of the experimentally undefined Zn-dominant IR and Raman spectral bands of this unusual Zn(I) species.

I. Background and Motivation

The predominant oxidation state for Zn is +2, unlike Hg which can be +1 or +2. Recently, Resa et al.[1] announced their synthesis of decamethyldizincocene, $Zn_2(\eta^5\text{-}C_5Me_5)_2$, an organometallic compound they hypothesized as Zn(I) formally derived from the dimetallic $[Zn-Zn]^{2+}$ unit. Their X-ray studies show that it contains two eclipsed $Zn(\eta^5\text{-}C_5Me_5)$ fragments with a Zn−Zn distance (± standard deviation) of 2.305(±3) Å, indicative of a metal−metal bonding interaction. However, they expressed some uncertainty about the presence of the direct Zn−Zn bonding. They also indicated their IR and Raman spectra provide no useful structural information. Our motivation in this work is to corroborate the experimental geometry as a true minimum on the global molecular energy surface, investigate the oxidation state of the Zn atoms, and identify the Zn-dominant IR and Raman spectral bands for potential future use in experimental studies of this type of Zn(I)-containing species.

II. Methodology

ArgusLab[2] was used to generate the initial geometrical model for the decamethyldizincocene species with this model being optimized using the PM3 approximation to the standard convergence limits specified within ArgusLab. Final geometry optimization and analysis was then performed using the pcGAMESS software package[3] to perform spin-restricted X3LYP[4] density functional theory calculations. Autogenerated delocalized coordinates and the internal GAMESS 6-31G* and TZVP GTO basis sets[3] were used to perform full geometry optimizations of decamethyldizincocene to the standard convergence limits specified within pcGAMESS. Initial pcGAMESS calculations were performed with the 6-31G* basis set. Final calculations and analysis were performed with the TZVP basis set.

Natural atomic charges (NACs) and bonding information were calculated using the natural bond orbital (NBO) method of Weinhold et al.[5]

Two-sided, translation- and rotation-projected, normal coordinate decomposition analysis was performed as implemented in pcGAMESS using a *z*-matrix generated from the optimized geometries. In order to better represent experimental results, all vibrational frequencies are scaled by a factor of 0.989, as suggested by Bauschlicher and Partridge[6] for a B3LYP triple-ζ basis set. The intrinsic frequency decomposition method of Boatz and Gordon[7] was used to determine the intrinsic force constant for the Zn−Zn bond.

A method to elucidate the contribution of the Zn atoms and their associated internal coordinates to the IR and Raman spectra of decamethyldizincocene is provided via the method of the total energy distribution matrix.[8] In the framework of the harmonic approximation, vibrational frequencies and normal coordinate displacements are determined by diagonalization of the mass-weighted Cartesian force constant matrix. Through simple transformations the following equation is obtained

$$\Lambda = D^{t}FD$$

where Λ is the diagonal matrix of the frequencies, D is the eigenvector matrix expressed in terms of internal coordinates, D^t is its transpose, and F is the corresponding force constant matrix. This can be written in scalar form

$$\lambda_i = \sum_m \sum_n D_{mi}F_{mn}D_{ni}$$

Then we can define the vibrational density matrix P^i as

$$P^i{}_{mn} = D_{mi}F_{mn}D_{ni}/\lambda_i$$

The total energy distribution matrix M is calculated from P_i via

$$M_{im} = \sum_n P^i{}_{mn} = \sum_n D_{mi}F_{mn}D_{ni}/\lambda_i$$

and represents the contribution of the *m*th internal coordinate to the energy of the *i*th normal mode.[9] Note

$$\sum_m M_{im} = 1$$

so that we can use the M_{im} to directly understand the fractional contribution of the *m*th internal coordinate to the *i*th vibrational mode.

WinGAM[10] was used to generate the graphical presentation of the calculated IR and Raman spectra. For this purpose we used the default values for the Lorentzian half intensity width (16 cm^{-1}) and intensity scale (1.0). All molecular schematics and 3D rendered orbital graphics were generated using ChemCraft.[11]

III. Results and Discussion

A. Structural Geometry and Bonding. A molecular schematic of decamethyldizincocene is displayed in Figure 1. Cp*

10.1021/jp051065x CCC: $30.25
Published on Web 08/06/2005

TABLE 1: Comparison of Essential Geometry Parameters

geometric parameter	X3LYP 6-31G*	X3LYP TZVP	B3LYP DZP[12]	BP86 DZP[12]	experiment
ZnB−ZνT−Cp* (deg)	179.9	179.4	180 (assumed)	180 (assumed)	177.4(±1)
ZnB−ZnT (Å)	2.29	2.32	2.336	2.315	2.305(±3)
ZnT−Cp* (Å)	1.87	1.96	1.97	1.949	2.04(±3)
ZnT−Cring (Å)	2.29	2.30	2.315	2.301	2.27-2.30(±3)

is the center point of a cyclopentadienal ring (Cp) and is only used for reference purposes.

A full geometry optimization was performed. Essential geometrical parameter information for the optimized geometries is listed in Table 1 along with a comparison with the experimental results. A complete set of optimized geometry Cartesian Coordinates and their associated *z*-matrix representations can be found in Supporting Information Tables 1S and 2S.

An examination of the wave function at the optimized geometry finds that the HOMO energy is negative, the LUMO energy is positive, and the HOMO/LUMO gap is significant, at 0.2 hartree. In addition, spin-unrestricted singlet calculations (single-point and geometry optimizations) were carried out with a mixing of α and β HOMO and LUMO orbitals so as to generate inequivalent α and β orbital spaces. The results showed no sign of spin contamination and were identical to the spin-restricted calculations. These results indicate a single-reference wave function is appropriate for this system.

The geometry optimization was not constrained by using symmetry since it is apparent from the experimental results that the complex is of C_s symmetry at best. Specifically, the slight deviation of the ZnB−ZnT−Cp* angle from 180°, the slight deviation from parallel orientation of the rings, as well as an unequal bifurcation of the C_{ring}−Cp*−C_{ring} angle by the plane defined by the ZnB−ZnT−Cp* atoms limits the possible point group of the molecule to C_s or C_1. We wanted to be sure no artificial symmetry constraints were placed on the optimization process and final results, so all optimization calculations were performed assuming a C_1 point group.[13]

The symmetry of the calculated result is C_s, and no imaginary frequencies were found at the optimized geometry, indicating it was a minimum and not a saddle point. The Cp rings are in an eclipsed conformation and nearly parallel, consistent with the experimental data.[14]

For both basis sets the agreement between experiment and theory for the ZnB−ZnT and ZnT−C_{ring} bond lengths falls within the deviation observed for the application of DFT methods, i.e., 0.02 Å RMS,[15] and the experimental error. The TZVP basis set does a better job for the ZnT−Cp* and ZnT−C_{ring} bonds than the 6-31G*.

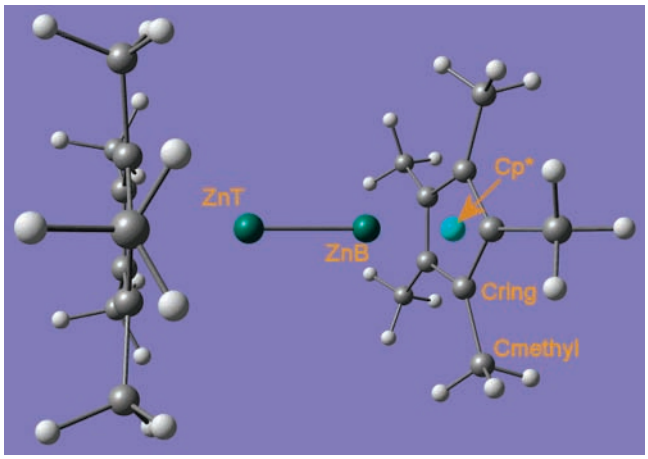

Figure 1. Molecular schematic.

TABLE 2: Energy Variation as a Function of ZnB−ZnT−Cp* Angle

ZnB−ZnT−Cp* (deg)	TZVP (kcal/mol)
174.44	0.14
179.44	0.00
185.44	0.11

TABLE 3: Energy Variation as a Function of ZnT−Cp* Bond Length

ZnT−Cp* bond length (Å)	TZVP (kcal/mol)
1.87	0.99
1.92	0.26
1.96	0.00
2.00	0.24
2.04	0.84
2.08	1.58

The agreement between experiment and theory for the ZnB−ZnT−Cp* angle falls slightly outside the deviation observed for the application of DFT methods, i.e., 1.4° RMS,[9] and the experimental uncertainty. However, it is interesting to note that the energy change as a function of the ZnB−ZnT−Cp* angle is quite flat over the range encompassing both the experimental and calculated equilibrium values (see Table 2); thus, the slight difference between the experimental and calculated results is not surprising.

The variation between the calculated ZnT−Cp* distance and the experimental result falls outside the expected quality of the DFT results. While the energy change as a function of this bond length is also flat over the range encompassing both the experimental and calculated equilibrium values (see Table 3), the source of this deviation between experiment and calculation is not clear.

Decamethyldizincocene is stable relative to a pair of zinc−pentamethylcyclopentadienyl species (i.e., decamethyldizincocene cleaved at the Zn−Zn bond) by 71.8 kcal/mol. Decamethyldizincocene is also stable relative to decamethylzincocene plus a zinc atom by 26 kcal/mol. Both results are consistent with the relative decomposition results reported by Resa et al.

B. Bonding Analysis. The Wiberg bond order for the Zn−Zn bond is 0.704, indicative of a single bond between the Zn atoms. The NBO analysis confirms the existence of a σ bond consisting of the bonding contributions between the 4s orbitals of each of the Zn atoms. This σ-bonding orbital has an occupancy of 1.9445. The intrinsic frequency decomposition method yields a Zn−Zn force constant of 0.0807 hartrees/b^2, roughly one-half of the Zn−C_{ring} value (0.172) and one-third the C_{ring}−C_{Me} value (0.251).

We also performed a Hoffmann fragment molecular orbital analysis (FMOA) to characterize the Zn bonding in more detail. The molecular orbitals were analyzed with AOMix[16,17] and NBO with a specific emphasis on only the orbitals directly involved in the Zn bonding. This included both the Zn−Zn bonding as well as the Zn−Cp* bonding.

There are three molecular orbitals in the decamethyldizincocene complex that have significant Zn bonding. They are orbitals 101, 95, and 59.

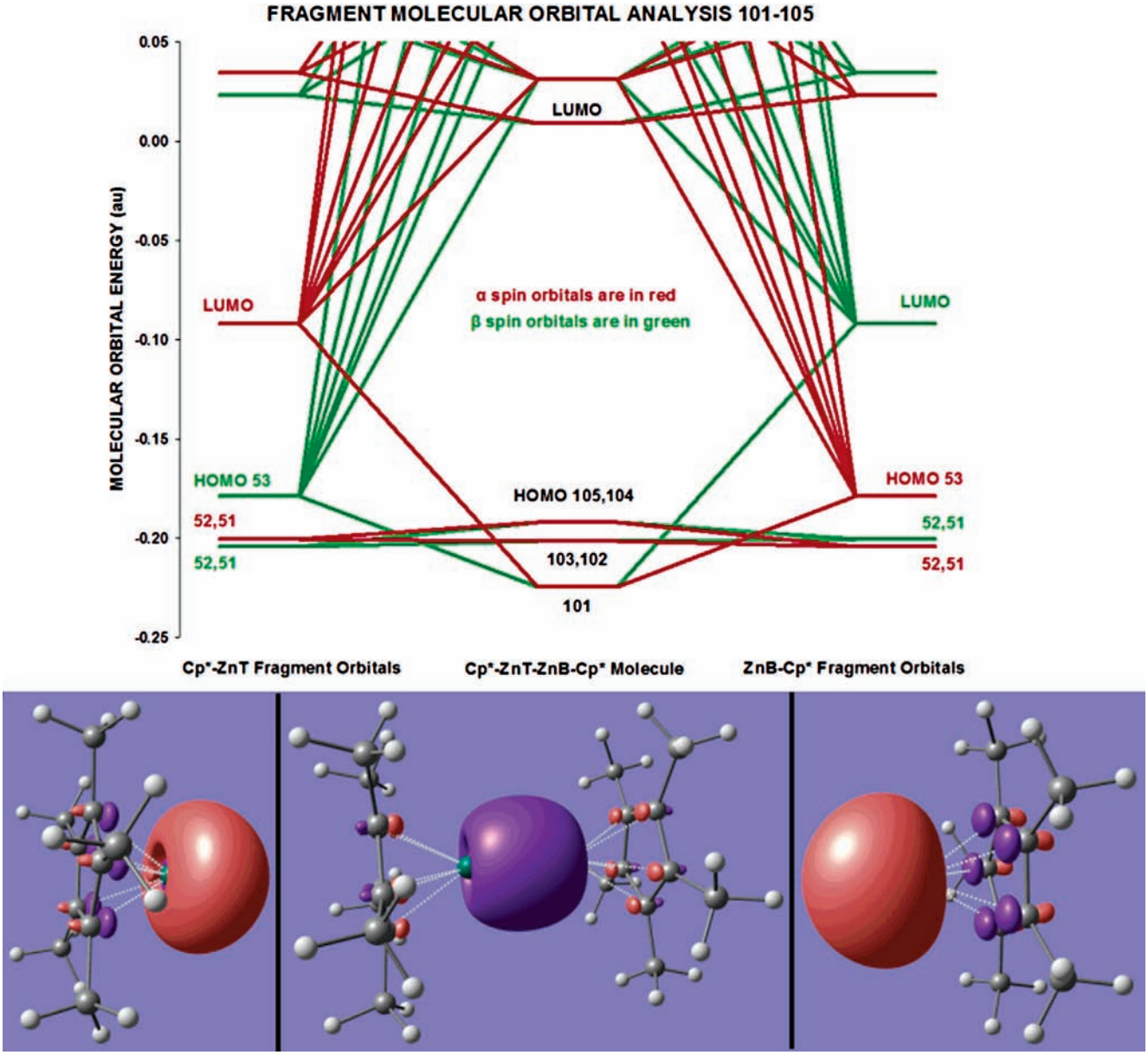

Figure 2. FMOA for MO 101.

As we can see in Figure 2, dizincocene molecular orbital 101 is formed by the combination of fragment orbitals 53 α and 53 β from both fragments.

A NBO analysis of the fragments indicates 53 α has 11% bonding character with 6% in the Cp* species. The 88% nonbonding character is focused primarily in the Zn atom (86%) as a singly occupied orbital. A NBO analysis of the fragments indicates 53 β has a 5% bonding character, a 28% nonbonding character (24% in the Zn atom), and 67% antibonding character (66% between the Zn and Cp* atoms).

A NBO analysis of the fragments indicates the dizincocene molecular orbital 101 has a 88% overall bonding character with 70% being between the Zn atoms, derived from the coupling of the singly occupied orbitals of the fragments, and 10% shared between the Cp* atoms. It has 4% nonbonding character and 8% antibonding character.

As we can see in Figure 3, dizincocene molecular orbital 95 is formed by the combination of fragment orbitals 48 α and 48 β from both fragments.

Forty-eight α has a 89% bonding character with 56% in the Cp* species and 15% between the Zn and Cp* atoms. The 9% nonbonding character is focused primarily in the Zn atom (6%). It also has 2% antibonding character. Forty-eight β has a 94% bonding character with 59% in the Cp* species and 20% between the Zn and the Cp* atoms. It also has 3% nonbonding character and 3% antibonding character.

Dizincocene molecular orbital 95 has a 93% overall bonding character with 9% being between the Zn atoms, 14% between the Zn and Cp* atoms, and 18% in the Cp* species. It has 5% nonbonding character and 2% antibonding character.

Finally, as we can see in Figure 4, dizincocene molecular orbital 59 is formed by the combination of fragment orbitals 30 α and 30 β from both fragments.

Thirty α has a 66% bonding character with 34% of that in the Cp* species. Thirty α also has a 34% nonbonding character focused primarily in the Zn atom (30%). Thirty β has a 70% bonding character with 37% in the Cp* species and 0% in the Zn atom. There is 30% nonbonding character, all of which is in the Zn atom.

Dizincocene molecular orbital 59 has a 53% overall bonding character with 6% being bonding between the Zn atoms and

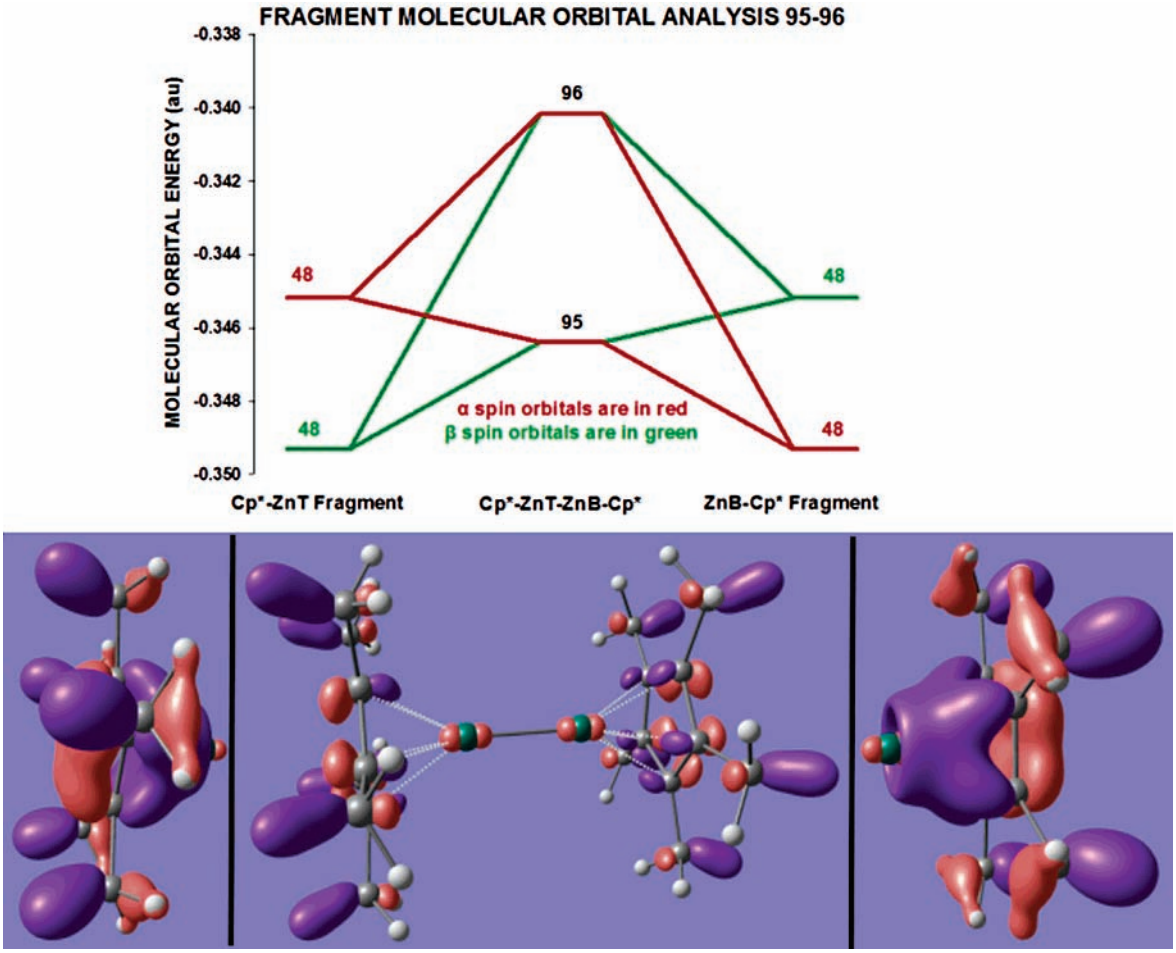

Figure 3. FMOA for MO 95.

the balance (47%) in the Cp* species. It has 46% nonbonding character, equally split between the Zn atoms.

C. Zn Oxidation State. Resa et al. hypothesized that the decamethyldizincocene complex is an example of a previously unobserved +1 oxidation state of Zn. Keeping in mind some simple definitions for oxidation state, "The number of electrons to be added (or subtracted) from an atom in a combined state to convert it to the elemental form" as well as "an alternate term that can be used when referring to the charge on an atom", we hypothesize that we can calculate an oxidation state surrogate using calculated atomic charges.

To establish the validity of this approach we first examined some known I and II Group 12 compounds of Hg and Zn to determine how we could use NACs to relate calculated atomic charges to the cation oxidation states. The geometry of all molecular species was optimized using TZVP basis sets and pcGAMESS as described previously. For molecules involving Hg we used the internal SBKJC effective core potentials and associated basis sets. The NACs were then calculated at these optimized geometries.

The results of our analysis are presented in Table 4. In both test cases, $Hg(I)_2Cl_2$ vs $Hg(II)Cl_2$ and $Zn(I)_2Cl_2$ vs $Zn(II)Cl_2$, we found that we could differentiate between the I and II states of the cation using the ratio of the NACs. Specifically, the ratio of NAC(II)/NAC(I) was approximately equal to the ratio of the oxidation states (i.e., 2/1) in both cases.

Applying this method to decamethyldizincocene ($Zn_2(C_5Me_5)_2$ in the table), using zincocene $Zn(C_5H_5)_2$ as the (II) cation reference we see from Table 4 that NAC(II)/NAC(I) = 1.69, thus indicating the Zn species in decamethyldizincocene is the I cation, as hypothesized by Resa et al.

TABLE 4: Oxidation State Analysis Results

molecule	formal oxidation state	NAC	NAC(II)/ NAC(I)
Hg_2Cl_2	I	0.645	1.68
$HgCl_2$	II	1.082	
Zn_2Cl_2[a]	I	0.720	1.86
$ZnCl_2$	II	1.336	
$Zn_2(C_5Me_5)_2$	I (?)	0.858	1.69
$Zn(C_5H5)_2$	II	1.452	

[a] Zn_2Cl_2 is a hypothetical species used to compare with the known species $ZnCl_2$ in a manner analogous to the Hg compounds.

D. Vibrational Analysis. We performed a vibrational analysis to provide some insight into the details of the infrared and Raman spectra of decamethyldizincocene, especially for those features that involve Zn bonding in the molecule. Table 5 and Figure 5 present the results of the IR analysis for Zn significant vibrational modes. The Supporting Information contains the complete results for this analysis (Hessian, dipole derivatives, and polarizability derivatives in Table 3S, total energy distribution matrix in Table 4S, normal modes in Cartesian coordinates, frequencies, IR intensities, Raman intensities, depolarization in Table 5S, and normal modes in internal coordinates in Table 6S).

It is interesting to note that the highest IR intensity absorption for all 150 vibrational modes (6.196) in Table 5 is associated with vibrational mode 41 (320.9 cm^{-1}) in which 10 $Zn-C_{ring}$ stretches and 10 $Zn-C_{ring}-C_{methyl}$ bends are the dominant internal coordinates with no obscuring $(CpMe_5)_2$ ligand absorp-

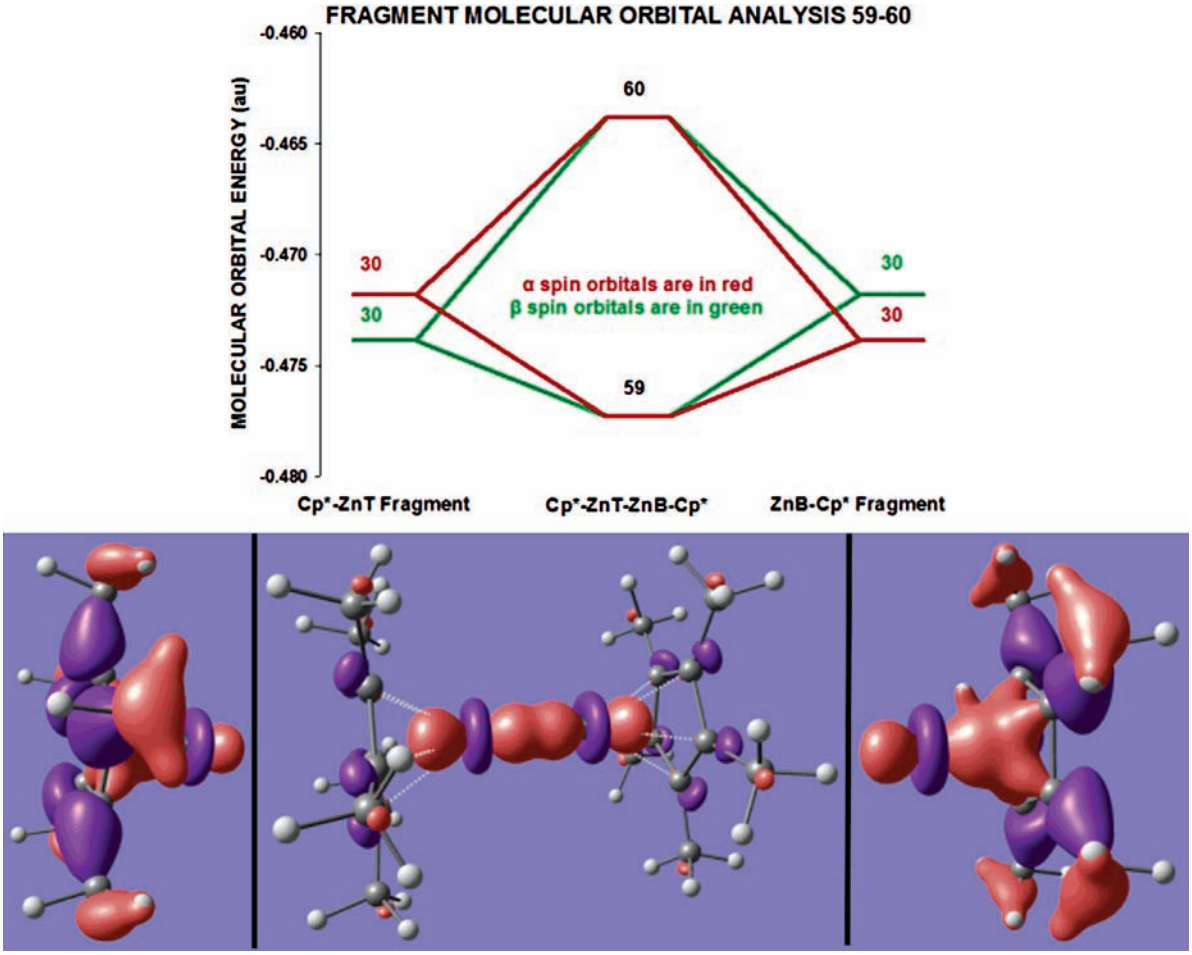

Figure 4. FMOA for MO 59.

TABLE 5: Results for Zn Significant Vibrational Modes with IR Intensity > 0.01[a]

mode	frequency	IR intensity	PCC	EDM PCC	PZnCC	EDMPZnCC	TZnCC
41	317.34	6.19568	STR.-CRT-ZnT	0.058	STR.-CRT-ZnT	0.058	0.975
91	1417.43	1.18120	STR.-CMB-CRB	0.032	BEND-CRT-ZnT-ZnB	0.031	0.436
53	586.77	0.24347	STR.-CMT-CRT	0.054	BEND-CRT-ZnT-ZnB	0.037	0.460
104	1461.05	0.19207	TORS-CRB-ZnB-ZnT-CRB	0.063	TORS-CRB-ZnB-ZnT-CRB	0.063	0.503
103	1460.85	0.19108	TORS-HT-CMT-CRT-HT	0.062	TORS-CRT-ZnT-ZnB-CRT	0.055	0.506
34	280.53	0.05673	TORS-CMT-CRT-ZnT-ZnB	0.189	TORS-CMT-CRT-ZnT-ZnB	0.189	0.949
36	282.15	0.05109	TORS-CMT-CRT-ZnT-ZnB	0.357	TORS-CMT-CRT-ZnT-ZnB	0.357	0.950
18	105.68	0.01286	TORS-CRB-ZnB-ZnT-CRB	0.211	TORS-CRB-ZnB-ZnT-CRB	0.211	0.999
17	103.59	0.01213	TORS-CRT-ZnT-ZnB-CRT	0.191	TORS-CRT-ZnT-ZnB-CRT	0.191	0.999

[a] PCC = principle contributing coordinate to this mode of the energy distribution matrix, EDM PCC = energy distribution matrix element for the PCC, PZnCC = principle Zn contributing coordinate to this mode of the energy distribution matrix, TZnCC = total of all Zn contributing coordinate energy distribution matrix elements for this mode, frequencies are in cm^{-1}, intensities are in D^2/amu-$Å^2$, EDM elements are dimensionless, STR are bond stretches, TORS are torsions, CRT/B, CMT/B, ZnT/B, HT/B = C_{ring}, C_{methyl}, Zn, H Top/Bottom.

tion (the total Zn coordinate contribution is 0.975). Modes 17, 18, 34, and 36 are similarly dominated by internal coordinates involving Zn, albeit with lower IR intensities. The Zn bonding and $(CpMe_5)_2$ ligand absorptions are equally dominant for modes 53, 91, 103, and 104. The other Zn contribution modes can be analyzed similarly using the information in the Supporting Information.

Table 6 and Figure 6 present the results of the Raman analysis for Zn significant vibrational modes.

The highest 14 intensity Raman absorptions are all dominated by $(CpMe_5)_2$ ligand absorptions with mode 136 having the highest intensity Raman absorption of all 150 vibrational modes. The highest intensity Zn dominated modes correspond to the Zn−Zn stretch (modes 46 and 12) and Zn−C_{ring}−C_{methyl} bends (modes 44 and 45). The Zn bonding and $(CpMe_5)_2$ ligand absorptions are equally dominant for modes 54, 92, 105, and 106. The other Zn contribution modes can be analyzed similarly using the information in the Supporting Information.

IV. Conclusions

In this work we have presented the results of a density functional investigation into the structure and vibrational properties of the recently synthesized, novel, Zn(I)-containing species, decamethyldizincocene. We confirmed that the published Resa et al. structure is a true minimum on the global molecular energy surface with good correspondence between experimental and calculated geometries. We also showed that the oxidation state of the Zn atoms in the molecule is I.

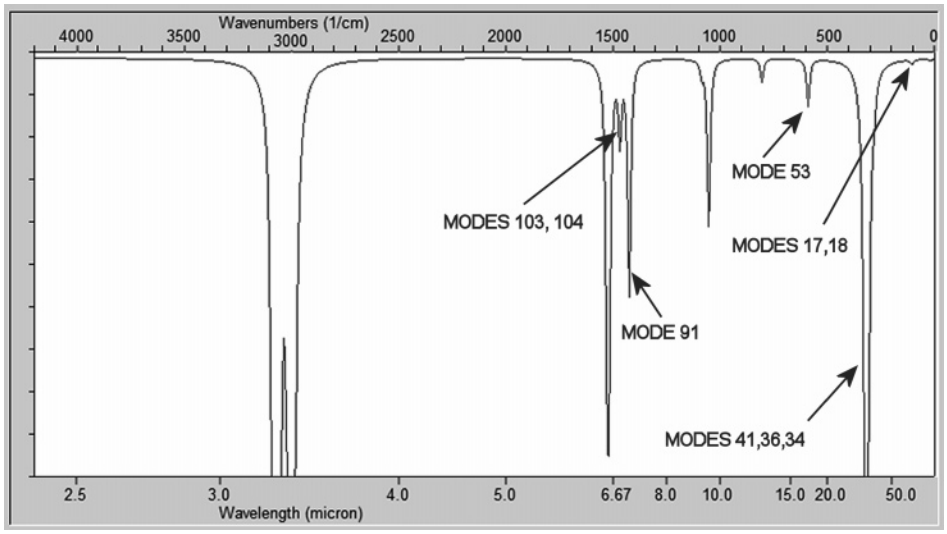

Figure 5. Computed IR spectrum.

TABLE 6: Results for Zn Significant Vibrational Modes with Raman Intensity > 10[a]

mode	frequency	Raman intensity	Dep	PCC	EDM PCC	PZnCC	EDM PZnCC	TZnCC
136	2986.58	1736.58	0.01	STR.-HB-CMB	0.181		0.000	0.000
92	1419.02	71.776	0.04	STR.-CMT-CRT	0.032	BEND-CRT-ZnT-ZnB	0.031	0.438
54	588.15	44.258	0.07	STR.-CMB-CRB	0.055	BEND-CRB-ZnB-ZnT	0.039	0.459
46	383.89	21.113	0.18	STR.-ZnB-ZnT	0.281	STR.-ZnB-ZnT	0.281	0.985
44	358.33	15.815	0.75	BEND-CMT-CRT-ZnT	0.098	BEND-CMT-CRT-ZnT	0.098	0.959
45	358.90	15.661	0.75	BEND-CMT-CRT-ZnT	0.108	BEND-CMT-CRT-ZnT	0.108	0.959
105	1461.64	11.395	0.75	TORS-HB-CMB-CRB-HB	0.063	TORS-CRT-ZnT-ZnB-CRT	0.054	0.500
106	1461.94	11.037	0.75	TORS-CRB-ZnB-ZnT-CRB	0.062	TORS-CRB-ZnB-ZnT-CRB	0.062	0.498
12	91.82	10.522	0.25	STR.-ZnB-ZnT	0.286	STR.-ZnB-ZnT	0.286	0.997

[a] Dep = depolarization, PCC = principle contributing coordinate to this mode of the energy distribution matrix, EDM PCC = energy distribution matrix element for the PCC, PZnCC = principle Zn contributing coordinate to this mode of the energy distribution matrix, TZnCC = total of all Zn contributing coordinate energy distribution matrix elements for this mode, frequencies are in cm^{-1}, intensities are in $Å^4$/amu, EDM elements are dimensionless, STR are bond stretches, TORS are torsions, CRT/B, CMT/B, ZnT/B, HT/B = C_{ring}, C_{methyl}, Zn, H Top/Bottom.

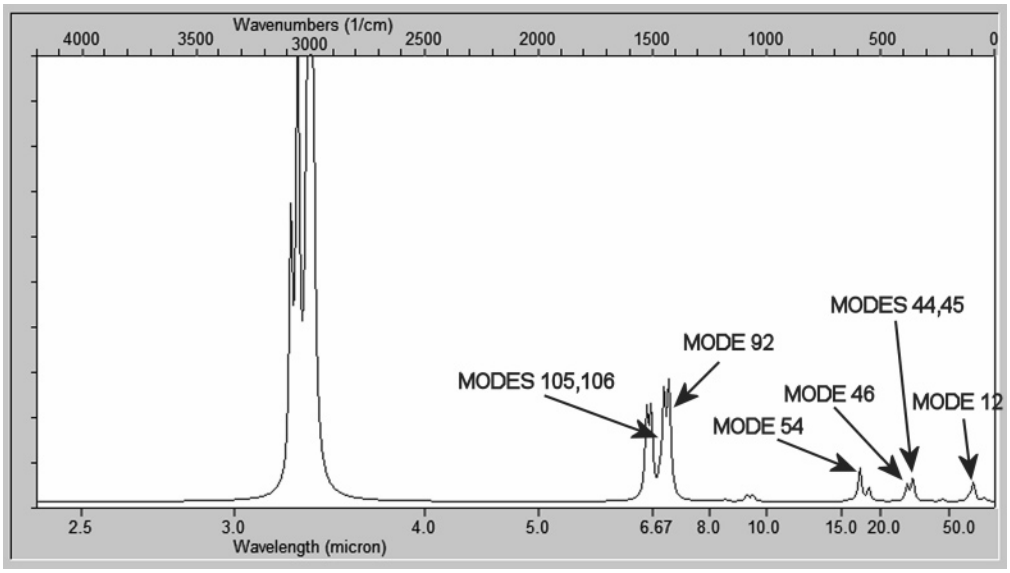

Figure 6. Computed Raman spectrum.

We determined that Zn-dominant IR absorptions should be observable at 317.34, 280.53, 282.15, 105.68, and 103.59 cm^{-1} with additional discernible Zn-related absorptions at 1417.43, 586.77, 1461.05, and 1460.85 cm^{-1}. With respect to Raman absorption, we find that Zn-dominant absorptions should be observable at 383.89, 358.33, 358.90, and 91.82 cm^{-1} with additional discernible Zn-related absorptions at 1419.02, 588.15, 1461.64, and 1461.94 cm^{-1}.

Acknowledgment. We thank Dr. Alexander Granovsky for access to the pcGAMESS program and many discussions regarding its application. We also thank Mark Thompson for his help with, and implementation of modifications to, ArgusLab for use in this work.

Supporting Information Available: Complete set of optimized geometry Cartesian coordinates and their associated

z-matrix representations (Tables 1S and 2S); complete vibrational analysis results (Hessian, dipole derivatives, and polarizability derivatives in Table 3S, total energy distribution matrix in Table 4S, normal modes in Cartesian coordinates, frequencies, IR intensities, Raman intensities, depolarization in Table 5S, and normal modes in internal coordinates in Table 6S). This material is available free of charge via the Internet at http://pubs.acs.org.

References and Notes

(1) Resa, I.; Carmona, E.; Gutierrez-Puebla, E.; Monge, A. *Science* **2004**, *305*, 1136.

(2) Thompson, M. A. *ArgusLab 4.0*; Planaria Software LLC: Seattle, WA; http://www.arguslab.com.

(3) Granovsky, A. A. www http://classic.chem.msu.su/gran/gamess/index.html. Schmidt, M. W.; Baldridge, K. K.; Boatz, J. A.; Elbert, S. T.; Gordon, M. S.; Jensen, J. H.; Koseki, S.; Matsunaga, N.; Nguyen, K. A.; Su, S.; Windus, T. L.; Dupuis, M.; Montgomery, J. A. *J. Comput. Chem.* **1993**, *14*, 1347−1363.

(4) Xu, X.; Goddard, W. A. *Proc. Natl. Acad. Sci. U.S.A.* **2004**, *101*, 2673.

(5) Glendening, E. D.; Badenhoop, J. K.; Reed, A. E.; Carpenter, J. E.; Weinhold, F. *NBO 4.M*; Theoretical Chemistry Institute, University of Wisconsin: Madison, WI, 1999.

(6) Bauschlicher, C. W.; Partridge, H. *J. Chem. Phys.* **1995**, *103*, 1788.

(7) Boatz, J. A.; Gordon, M. S. *J. Phys. Chem.* **1989**, *93*, 1819.

(8) Pulay, P.; Torok, F. *Acta Chim. Acad. Sci. Hung.* **1966**, *47*, 273.

(9) Morpurgo, S.; Bossa, M.; Morpurgo, G. O. *Phys. Chem. Chem. Phys.* **2001**, *3*, 4898.

(10) winGAM, Ernst Schumacher, Chemsoft.ch, http://chemsoft.ch/.

(11) Zhurko, G. A. ChemCraft program, http://www.chemcraftprog.com/.

(12) Xie, Y.; Schaefer, H. F.; King, R. B. *J. Am. Chem. Soc*. **2005**, *127*, 2818.

(13) A full geometry optimization plus double-sided, projected vibrational analysis was performed using C_{5h} symmetry and the 6-31G* basis set. The results provided one imaginary frequency indicating the C_{5h} optimized geometry was a saddle point, not a true minimum.

(14) Cambridge Crystallographic Data Centre CIF file CCDC 233010.

(15) Young, D. *Computational Chemistry, A Practical Guide for Applying Techniques to Real World Problems*; Wiley & Sons: New York, 2001; pp 137−142.

(16) Gorelsky, S. I. *AOMix* program, http://www.sg-chem.net/.

(17) Gorelsky, S. I.; Lever, A. B. P. *J. Organomet. Chem.* **2001**, *635*, 187−196.